remote sensing

MDPI

Article

Quantifying the Effect of Land Use and Land Cover Changes on Spatial-Temporal Dynamics of Water in Hanjiang River Basin

Hao Xi, Yanbin Yuan, Heng Dong and Xiaopan Zhang *

School of Resource and Environmental Engineering, Wuhan University of Technology, Wuhan 430070, China; xihao289357@whut.edu.cn (H.X.); yuanyanbin@whut.edu.cn (Y.Y.); simondong@whut.edu.cn (H.D.)
* Correspondence: tom_xp@whut.edu.cn

Abstract: As a vital part of the geo-environment and water cycle, ecosystem health and human development are dependent on water resources. Water supply and demand are influenced significantly by land use and cover change (LUCC) which shapes the surface ecosystems by altering their structure and function. Under future climate change scenarios, LUCC may greatly impact regional water balance, yet the impact is still not well understood. Therefore, examining the spatial relationship between LUCC and water yield services is crucial for optimizing land resources and informing sustainable development policies. In this study, we focused on the Hanjiang River Basin and used the patch-generating land use simulation (PLUS) model, coupled with the Integrated Valuation of Ecosystem Services and Tradeoffs (InVEST) model, to assess water yield services under three Shared Socioeconomic Pathway and Representative Concentration Pathway (SSP-RCP) scenarios. For the first time, we considered the impact of future changes in socio-economic and water use indicators on water demand using correction factors and ARIMA projections. The relationship between water supply and demand was explored using this approach, and LUCC's effects on this balance are also discussed. Results indicate that: (1) The patterns of LUCC are similar for the three scenarios from 2030 to 2050, with varying levels of decrease for cropland and significant growth of built-up areas, with increases of 6.77% to 19.65% (SSP119), 7.66% to 22.65% (SSP245), and 15.88% to 46.69% (SSP585), respectively, in the three scenarios relative to 2020; (2) The future supply and demand trends for the three scenarios of produced water services are similar, and the overall supply and demand risks are all on a downward trend. Water demand continues to decline, and by 2050, the water demand of the 3 scenarios will decrease by 96.275×10^8 t, 81.210×10^8 t, and 84.13×10^8 t relative to 2020, respectively; while supply decreases from 2030 to 2040 and rises from 2040 to 2050; (3) Both water supply and demand distributions exhibit spatial correlation, and the distribution of hotspots is similar. The water supply and demand are well-matched, with an overall supply-demand ratio greater than 1.5; (4) LUCC can either increase or decrease water yield. Built-up land provides more water supply compared to other land types, while forest land has the lowest average water supply. Limiting land use type conversions can enhance the water supply.

Keywords: multi-source remote sensing; LUCC; water supply and demand risk; SSP-RCP; multi-scenario projection

check for updates

Citation: Xi, H.; Yuan, Y.; Dong, H.; Zhang, X. Quantifying the Effect of Land Use and Land Cover Changes on Spatial-Temporal Dynamics of Water in Hanjiang River Basin. *Remote Sens.* **2024**, *16*, 4136. https://doi.org/10.3390/rs16224136

Academic Editors: Yi Wang, Xiaohui Huang, Wei Han and Jining Yan

Received: 31 August 2024
Revised: 1 November 2024
Accepted: 1 November 2024
Published: 6 November 2024

Copyright: © 2024 by the authors. Licensee MDPI, Basel, Switzerland. This article is an open access article distributed under the terms and conditions of the Creative Commons Attribution (CC BY) license (https://creativecommons.org/licenses/by/4.0/).

1. Introduction

The geologic environment, which interacts with the atmosphere, hydrosphere, and biosphere, is an indispensable resource for the survival of humankind and economic development [1]. However, with rapid population and socio-economic growth, a range of environmental issues, including diminishing natural resources, rising pollution, and ongoing degradation, are occurring frequently, seriously constraining the sustainable development of human society [2,3]. Thus, monitoring the geo-environment is crucial. Remote sensing satellites offer extensive, high-resolution images with both temporal and spatial detail [4], and their usability has been increasing with the continuous progress of multi-source RS

image processing and application methods [5–7]. These images can be used to monitor the geologic environment, providing an efficient and high-precision method for geologic environment investigation and monitoring work [8–10], which is crucial for assessing the distribution and changes in natural resources and advancing sustainable human development [11].

Integral to the geo-environment, water resources are crucial for both ecosystem health and human sustenance [12]. The spatial differences within ecosystems often cause mismatches in water supply and demand [13]. Rapid urbanization and industrialization further strain water systems, leading to challenges such as flooding, water scarcity, and ecological degradation [14]. Effectively managing water resources requires a clear understanding of these imbalances [15], while detailed spatial and temporal analyses can pinpoint that.

As human-water system research advances, it's important to understand that balancing water supply and demand goes beyond mere resource scarcity; it involves the complexities of human-water interactions [16]. LUCC significantly influences this balance by altering both the distribution and timing of water availability and usage [17]. LUCC affects the hydrological cycle by altering runoff, soil moisture, groundwater recharge, and surface evapotranspiration [18,19]. Additionally, LUCC significantly impacts how water is allocated for production, ecological purposes, and domestic needs [20]. Analyzing historical and future LUCC trends and their characteristics is crucial for this study. Models such as PLUS predict future LUCC by incorporating socioeconomic and environmental factors [21,22], which helps in the development and coordination of human-land systems [23]. However, many studies on future land use do not consider future climatic and socioeconomic factors.

In this study, we focused on LUCC as the main driver of water supply and demand in the Hanjiang River Basin, a crucial source for China's water diversion projects. By integrating multi-source geo-environmental data, we analyzed the spatial-temporal dynamics of water supply and demand and employed a heat map to visualize their response to LUCC, showcasing a novel approach. The PLUS model was used to simulated future LUCCs, and water supply and demand were projected using the InVEST model and the quota method. A significant advancement of this research is the utilization of climatic and socioeconomic prediction data under three SSP-RCP scenarios. Notably, the socio-economic data derived from linear forecasting and ARIMA time series analysis is presented here for the first time, addressing the limitations of previous studies and enhancing the realism of the predictions.

2. Study Area and Data Processing Overview

2.1. Study Area

The Hanjiang River Basin, situated between 106°5′∼114°17′E and 30°4′∼34°12′N, is a key political, economic, cultural, and ecological hub in central China. It spans 20 districts across six provinces and municipalities: Hubei, Shaanxi, Henan, Sichuan, Chongqing, and Jiangxi, covering an area of 159,000 km^2 (Figure 1). The research region is characterized by a typical subtropical monsoon climatic zone, the annual precipitation mainly relies on flood season precipitation, and the average annual precipitation for many years is about 700∼1400 mm. Concentrated rainfall and uneven water distribution, with more in the southeast and less in the northwest, cause frequent floods and droughts, underscoring the urgent need for spatial analysis of water supply and demand to enhance resource utilization. Currently, four water transfer projects have been implemented in the Hanjiang River Basin, with annual transfer volumes of 9.5 billion m^3 for the South-to-North Water Transfer Project, 1.5 billion m^3 for the Hanjiang-Weihe Water Transfer Project, 3.1 billion m^3 for the Changjiang-Hanjiang Water Transfer Project, and 0.77 billion m^3 for the Hubei Province Water Transfer Project, which have alleviated supply-demand conflicts to some extent [24].

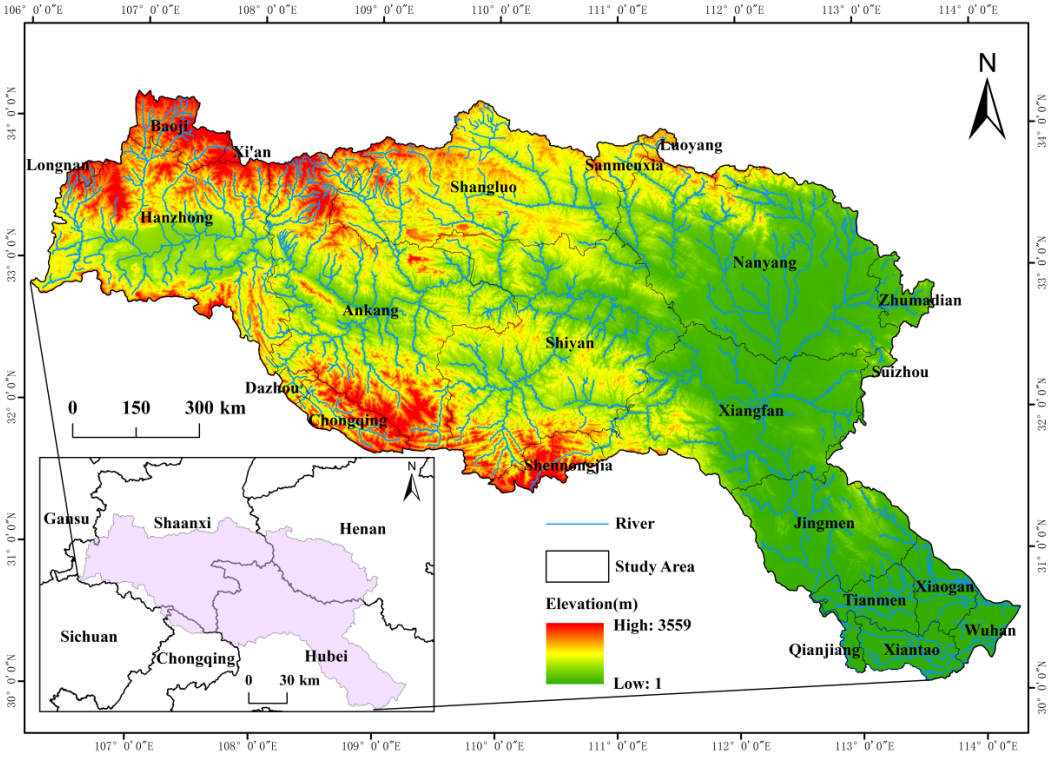


Figure 1. Hanjiang River Basin Study Area Map.

2.2. Sources and Preprocessing of Data

The 30 m spatial resolution land use data for 2000, 2010, and 2020 come from the Resource and Environmental Science Data Center. There are 6 major land use types in the dataset: cropland, forest, grassland, water body, built-up land, and barren, which are further divided into 25 subclasses. The secondary classification's overall accuracy is more than 90% [25]. In this study, We selected a total of 12 driving factors from four aspects: socio-economics, accessibility, climate, and topography for the land expansion module of the PLUS model. These factors have been commonly used in previous studies [26,27]. Among the economic factors, GDP and POP were chosen as the two driving factors, representing the intensity of human activities, which in turn influence LUCC. For accessibility factors, we selected six factors based on the shortest distances to trunk roads, primary roads, residential areas, highways, railways, and rivers, calculated using Euclidean distance from 2020 shapefile data obtained from OpenStreetMap. Shorter distances make it easier for land use types to change. The climate factors included the annual average temperature and total annual precipitation, while the topography factors included Digital Elevation Model (DEM) and slope. These factors influence LUCC by affecting surface water flow and vegetation growth. All multi-source raster data were processed with a uniform 100 m resolution resampling, and the month-by-month data were summed to annual data, ensuring consistency in both temporal and spatial resolutions, with the projection coordinate system standardized to "WGS 1984 UTM Zone 49N".

In predicting future land use changes, accessibility and topography factors are considered constant, while future socio-economic and climate factors corresponding to the prediction years are obtained through linear regression and existing multi-scenario climate prediction datasets. The specific sources of factor data are shown in Table 1. The driving factors for land expansion in the Hanjiang River Basin in 2020 are illustrated in Figure 2. In the InVEST model, in addition to the precipitation and LUCC data in Table 1, we require evapotranspiration, bedrock depth, and soil characteristic data for calculating soil moisture. We also require water use indicator data for estimating water demand. Table 2 provides the sources of these additional variables.

Table 1. Data sources on factors impacting the geographical distribution of LUCCs.

Type	Data	Unit	Spatial and Temporal Resolution	Source
Land Use Type	Land Use Type	-	Annual, 1 km	Resource and Environment Science and Data Center (accessed on 17 May 2024) (https://www.resdc.cn/)
Socio-economic Factors	Population Density	person/km^2	Annual, 1 km	East View Cartographic (accessed on 17 May 2024) (https://landscan.ornl.gov/)
	GDP	10,000 CNY/km^2	Annual, 1 km	Resource and Environment Science and Data Center (accessed on 17 May 2024) (https://www.resdc.cn/)
Accessibility Factors	Distance to 6 Road Network Elements	-	100 m	Open Street Map (accessed on 17 May 2024) (https://www.openstreetmap.org/)
Climate Factors	Annual Mean Temperature	°C	Annual, 1 km	National Earth System Science Data Center (accessed on 17 May 2024) (https://www.geodata.cn/)
	Annual Total Precipitation	mm	Annual, 1 km	National Earth System Science Data Center (accessed on 17 May 2024) (https://www.geodata.cn/)
	Future Multi-Scenario Annual Mean Temperature	°C	Annual, 1 km	National Earth System Science Data Center (accessed on 17 May 2024) (https://www.geodata.cn/)
	Future Multi-Scenario Annual Total Precipitation	mm	Annual, 1 km	National Earth System Science Data Center (accessed on 17 May 2024) (https://www.geodata.cn/)
Topographic Factors	Elevation (DEM)	m	30 m	Google Earth Engine (accessed on 17 May 2024) (https://code.earthengine.google.com/)
	Slope	degrees	30 m	Derived from DEM data

Table 2. Additional variables.

Data	Unit	Spatial and Temporal Resolution	Source
Soil Characteristics	-	-, 1 km	National Tibetan Plateau Data Center (accessed on 17 May 2024) (https://www.tpdc.ac.cn/)
Bedrock Depth	-	-, 100 m	Sun Yat-sen University Land-Atmosphere Interaction Research Group (accessed on 17 May 2024) (http://globalchange.bnu.edu.cn/)
Potential Evapotranspiration	mm	Annual, 1 km	National Earth System Science Data Center (accessed on 17 May 2024) (https://www.geodata.cn/)
Future Multi-Scenario Potential Evapotranspiration	mm	Annual, 1 km	National Earth System Science Data Center (accessed on 17 May 2024) (https://www.geodata.cn/)
Per Capita Household Water Use	m^3	Annual, -	Hubei Provincial Water Resources Bulletin (accessed on 17 May 2024) (https://slt.hubei.gov.cn/) Shaanxi Provincial Water Resources Bulletin (accessed on 17 May 2024) (http://slt.shaanxi.gov.cn/) Henan Provincial Water Resources Bulletin (accessed on 17 May 2024) (https://slt.henan.gov.cn/)
Water Use per 10,000 CNY GDP	m^3	Annual, -	as above
Water Use per Mu of Cropland Irrigation	m^3	Annual, -	as above

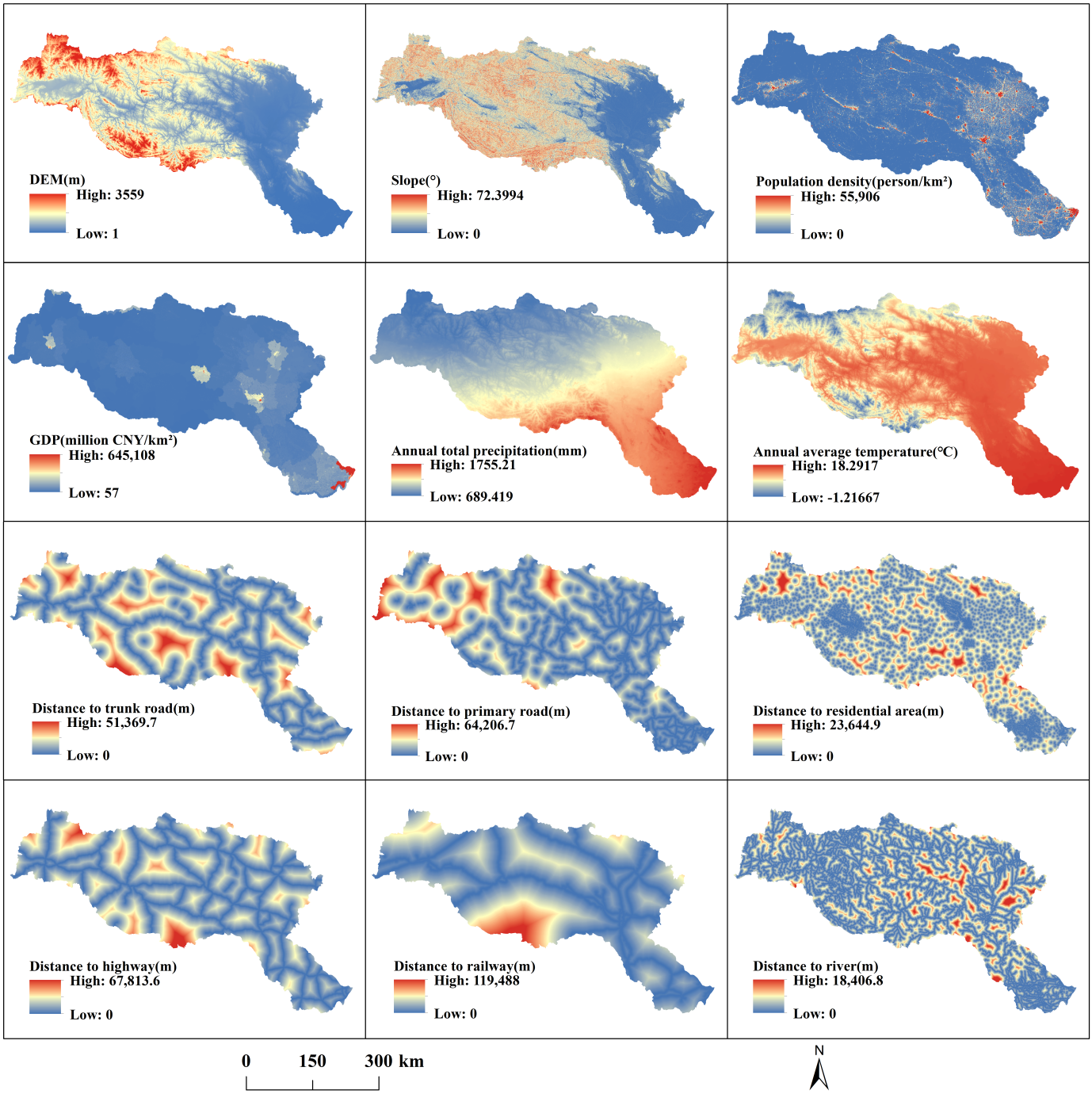


Figure 2. LUCC drivers in the Hanjiang River Basin.

3. Methods

The study framework consists of four main components, as illustrated in Figure 3. First, the Markov-PLUS model simulates and predicts LUCC according to various scenarios for the Hanjiang River Basin. Next, the InVEST model and quota method are adopted to estimate the water supply and demand across three scenarios (SSP119, SSP245, SSP585) (blue and yellow parts). Last, the supply-demand risk framework is used to assess the corresponding risks. In the demand prediction section, the impacts of changes in climate, industry coefficients (water use indicators), population, and GDP on future water demand under different SSP-RCP scenarios are considered for the first time. Additionally, the paper analyzes how LUCC influences water yield service supply.

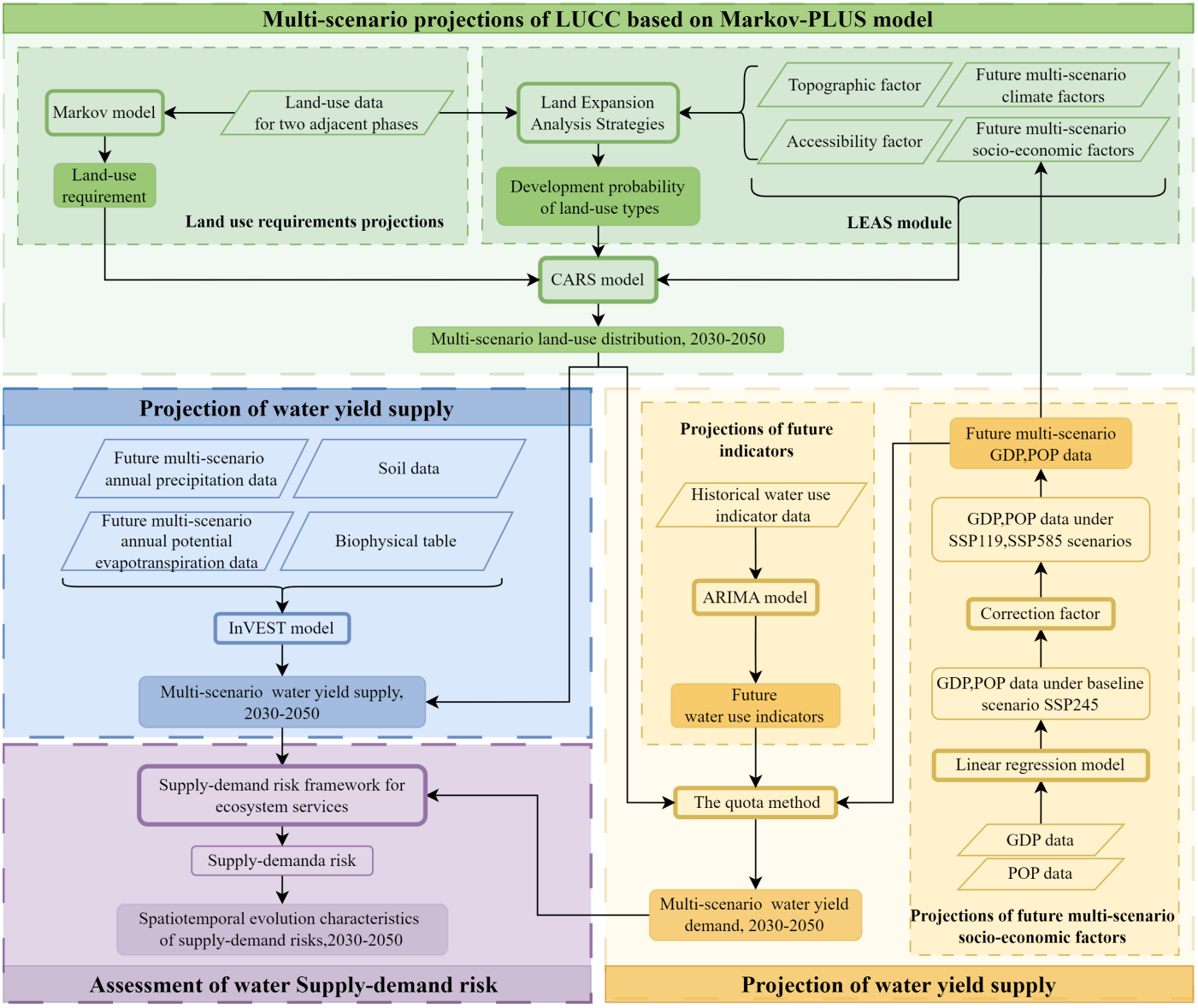


Figure 3. Risk assessment framework for water supply and demand.

3.1. Calculation of Water Supply and Demand

3.1.1. Supply of Water Yield Services

The supply of water yield service, which is essential for the ecohydrological cycle, depends on both precipitation and evapotranspiration. The widely used InVEST model [13,28,29] is utilized to determine the supply. The following are the core formulas:

$$Y_{(x)} = (1 - \frac{AET_{(x)}}{P_{(x)}}) \times P_{(x)} \quad (1)$$

$$\frac{AET_{(x)}}{P_{(x)}} = 1 + \frac{PET_{(x)}}{P_{(x)}} - \left[1 + \left(\frac{PET_{(x)}}{P_{(x)}}\right)^{\omega}\right]^{1/\omega} \quad (2)$$

$$w_{(x)} = Z \times (AWC_{(x)}/P_{(x)}) \quad (3)$$

For the pixel x, the annual water yield $Y_{(x)}$ is calculated as the difference between annual precipitation $P_{(x)}$ and actual evapotranspiration $AET_{(x)}$, with $PET_{(x)}$ representing the potential evapotranspiration. Additionally, w is an empirical parameter. The parameter Z represents the seasonal factor, which we can adjust to ensure that the simulated water

yield coefficient in the study area aligns with the coefficient reported in the water resources bulletin, thereby ensuring accuracy. The water yield coefficient is the ratio of water yield to precipitation. Using the area-weighted average method (detailed in Section 3.1.2 item (3)), we calculated the water yield coefficient for the Hanjiang River Basin to be 0.3793. After several adjustments, we set Z to 3.08 to equalize the coefficients, allowing it to accurately represent the actual water yield.

$$AWC_{(x)} = min(MaxSoilDepth_{(x)}, RootDepth_{(x)}) \times PAWC_{(x)} \quad (4)$$

$$PAWC_{(x)} = 54.509 - 0.132SAND_{(x)} - 0.003(SAND_{(x)})^2 - 0.055SILT_{(x)} - 0.006(SILT_{(x)})^2 - 0.738CLAY_{(x)} + 0.007(CLAY_{(x)})^2 - 2.699OM_{(x)} + 0.501(OM_{(x)})^2 \quad (5)$$

For the pixel x, the effective water content AWC_x is the product of the minimum of $MaxSoilDepth_x$ and $RootDepth_x$ with $PAWC(x)$. The $PAWC_x$ is calculated using the soil's sand content $SAND_x$, silt content $SILT_x$, clay content $CLAY_x$, and organic matter content OM_x.

3.1.2. Demand of Water Yield Services

Due to the severe restrictions imposed by government policies on accessing water use data, we referred to the ARIES model [30] to determine the spatial distribution of water demand. The quota method is employed for three water use categories: domestic, industrial, and agricultural using the formula listed as below [20]:

$$WD_{(i,j)} = pop_{(i,j)} \times l_i + gdp_{(i,j)} \times m_i + agr_{(i,j)} \times n_i \quad (6)$$

For the pixel j, $pop_{i,j}$, $gdp_{i,j}$, and $agr_{i,j}$ represent the population size, GDP, and cropland area in year i, respectively. Additionally, l_i, m_i, and n_i denote per capita residential water use, water use per 10,000 CNY of GDP, and water use per mu of cropland irrigation in year i.

(1) Multi-scenario socio-economic data forecasting based on linear regression modeling
The SSP245 scenario illustrates a future with moderate greenhouse gas emissions and intermediate progress in development, serving as the "baseline" world, whose technical, social, and economic changes mostly follow historical tendencies. Therefore, we used linear regression to project population and GDP for the SSP245 baseline scenarios in 2030, 2040, and 2050, based on data from 2000 to 2020. The projections showed high accuracy, achieving R-squared values of 0.93 and 0.86. Then the population and GDP data of the benchmark scenario are corrected by multiplying the correction factor to obtain the future population and GDP data of the SSP119 and SSP585 scenarios. About the principle of obtaining the correction factor: it is known that there are different LUCC patterns in different SSP-RCP scenarios, and because there are big differences in population density and average GDP in different land use types, the total population and GDP will change, resulting in the corresponding total population and GDP in different SSP-RCP scenarios will change, so the magnitude of this change is taken as the change factor. For example, the SSP245 scenario in year i is the baseline scenario, and its total population is POP_i. Assuming that the population density of its land type does not change in different scenarios, the total population is calculated based on the LUCC in different scenarios and is denoted as POP'_i. Using $\frac{\mathrm{POP}'_i}{\mathrm{POP}_i}$ to obtain the correction factor a, which is used to portray its magnitude of change, in the SSP245 base scenario, $a \times \mathrm{POP}_{(i,j)}$, thus realizing the correction of the population data of the base scenario, and similarly obtaining the GDP data of the different scenarios in the future.

(2) Multi-scenario cropland area prediction based on Markov-PLUS modeling
The Markov model captures changes in land use areas but lacks spatial attributes, while the PLUS model integrates existing land use with influencing factors for better spatial representation. This coupling allows us to perform a multi-scenario simulation of LUCC. Therefore, we employed the Markov-PLUS model to simulate cropland distributions for 2030 to 2050 under three scenarios. For example, agr_j is 15 if the pixel j is cropland; otherwise, it is 0, since each pixel covers 10,000 m^2 (15 mu).

(3) Forecasting water use indicators based on ARIMA time series modeling
For the prediction of water use indicators, we sourced historical water use indicator data exclusively from the water resources bulletins of Henan, Hubei, and Shaanxi, because they provide about 127,853 square kilometers of the Hanjiang River Basin, making up almost 82% of the entire region. The Autoregressive Integrated Moving Average (ARIMA) model was employed for prediction due to its simple structure, rapid modeling speed, and high accuracy [31]. Through many experiments, the (p, d, q) parameter of the ARIMA model was set to $(1, 1, 1)$. The prediction results are shown in Figure 4 below. Among them, the RMSE values for the three indicators (per capita water use for residential life, water use for 10,000 CNY GDP, and water use per mu of cropland irrigation) for Henan Province are 19.91, 129.15, and 21.13, respectively; for the three indicators for Hubei Province are 22.53, 232.85, and 60.52, respectively; and for the three indicators for Shaanxi Province are 6.29, 65.91, 21.48; because of the amount of historical data only 22 years, resulting in the prediction of the results of the RMSE value is larger, the simulation accuracy is general, but compared with other methods using the average value of the historical indicator or latest bulletin indicator value, and so on, and did not take into account the trend of the industry coefficients, it is more reasonable.

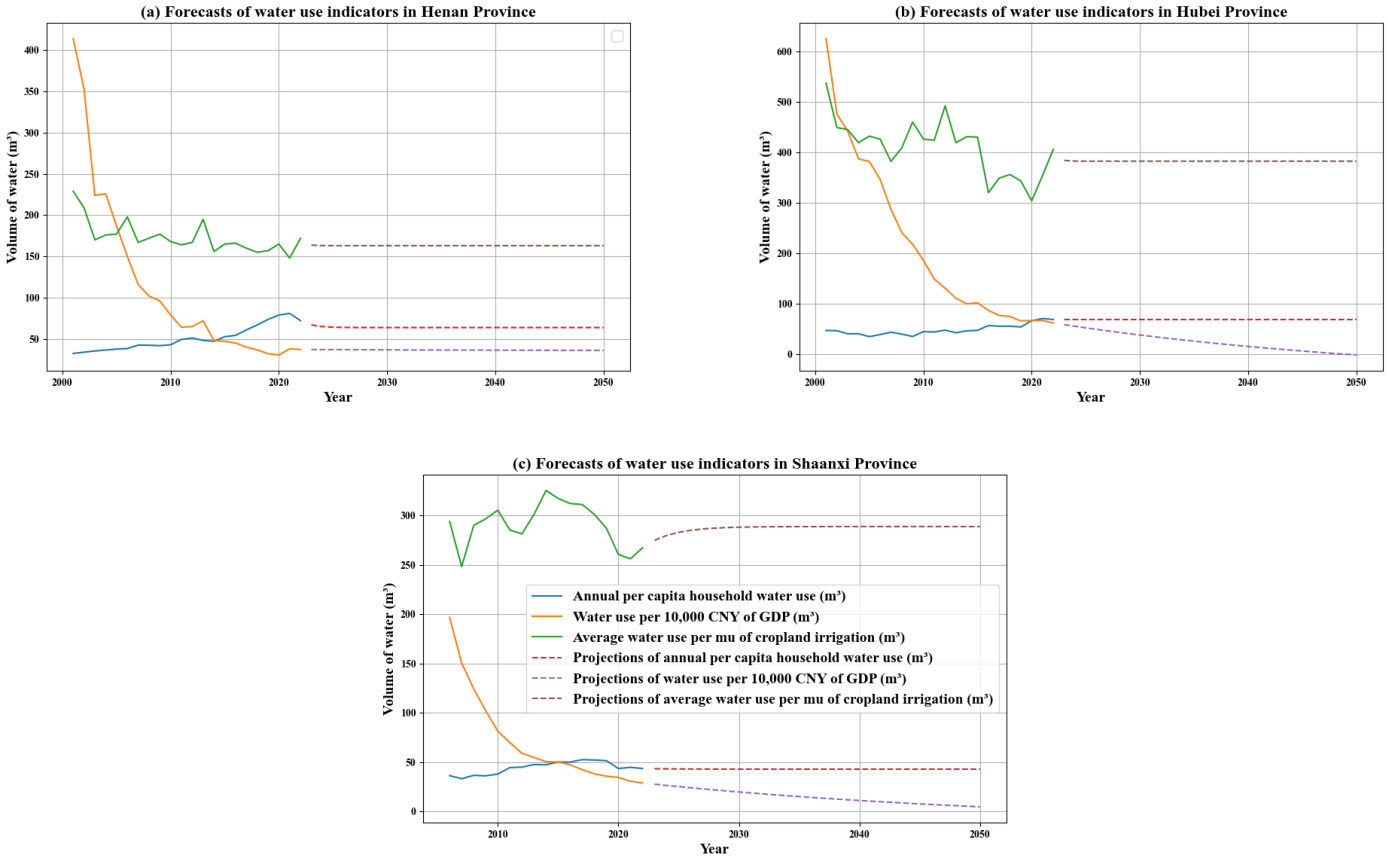


Figure 4. Projected Water Use Indicators.

As can be seen from Figure 4, the regional differences of the indicators are reduced and tend to be consistent, so the occupied area of Hanjiang River Basin in the three provinces is used as the weighting, in which the weights of Henan, Hubei, and Shaanxi are 0.179, 0.404, and 0.417, respectively, and the weighted average of the predicted indicators of the three provinces (presented in Table 3) is calculated to serve as the water consumption indicator of Hanjiang River Basin as a whole.

Table 3. Water Use Indicators from 2000 to 2050.

Water Use Indicators	2000	2010	2020	2030	2040	2050
Per Capita Household Water Use (m^3)	39.92	41.69	59.26	57.19	57.18	57.18
Water Use per 10,000 CNY GDP (m^3)	522.12	123.25	46.96	30.33	17.48	7.98
Water Use per Mu of Cropland Irrigation (m^3)	378.99	329.49	260.97	303.78	304.06	304.06

3.2. Markov Model

In a Markov model, a system's evolution is represented as a series of discrete states, and the probabilities of intertransitions between these states are described by a probability transfer matrix. Therefore, it is commonly used to predict an event's future state based on its current state [32].

3.3. PLUS Model

The PLUS model combines the Land Expansion Analysis Strategy (LEAS) and the Cellular Automata (CA) model [26]. The LEAS module uncovers the relationships between the expansion of different land use types and their driving factors, providing development probabilities for each type. Its built-in Random Forest Classification (RFC) model excels in feature selection and managing complex non-linear relationships in multi-source data, effectively reducing non-linear errors due to data diversity [33]. CA generates land patches based on these probabilities using a conversion matrix that indicates whether land use changes are allowed, where 0 denotes that conversion is forbidden and 1 denotes that conversion is possible. This study applies the model to the Hanjiang River Basin for the period 2000–2020, setting conversion rules below (Table 4).

Table 4. Conversion Cost Constraints Matrix.

LULC	Croplands	Forests	Grasslands	Water Body	Built-Up Lands	Barren
Croplands	1	1	1	1	1	1
Forests	1	1	1	1	1	1
Grasslands	1	1	1	1	1	1
Water body	0	0	0	1	0	0
Built-up lands	0	0	0	0	1	0
Barren	1	1	1	1	1	1

3.4. Future Climate Scenario Setting Based on CMIP6

The Coupled Model Intercomparison Project (CMIP), now in its sixth phase, is a leading international initiative in climate research. It has revolutionized climate science and supported both national and global climate change assessments. Building on CMIP5, CMIP6 introduces new projection scenarios, SSP-RCPs, derived from recent anthropogenic emission trends and various shared socio-economic pathways [34,35].

3.4.1. Scenario Description

SSP245 continues existing trends, SSP119 is a scenario focused on major emission reductions, and SSP585 denotes a scenario with high emissions. The land use number of 6 types in the Hanjiang River Basin for 2030–2050 was estimated using Markov chains based on trends from 2000 to 2020, with 10-year intervals. Spatial simulations were con-

ducted with CARS as the model's input parameter, with different scenarios using varying parameters. Future temperature, precipitation, GDP, and population were incorporated for control based on the chosen SSP-RCP scenarios. Finally, corresponding land expansion probabilities are assigned for three scenarios to simulate land use development. In SSP245, the original Markov transition matrix is applied. In SSP119, the probability of grassland and forest being converted to built-up land decreases by 30%, while the chances of built-up land reverting to these areas increase by 20%. SSP585 adjusts the probabilities by reducing the conversion from built-up land by 30% and increasing the reverse transition by 20%.

3.4.2. Driving Factor Acquisition

Most studies focus only on current factors, but this study includes four dynamic drivers—future temperature, precipitation, population, and GDP—under climate change scenarios. Future temperature and precipitation data come from the MRI-ESM2-0 model [36]. Section 3.1.2 obtained future population and GDP under different scenarios.

3.4.3. Neighborhood Weights Setting

Neighborhood weights, which range from 0 (no influence) to 1 (great impact), show how each form of land use affects the neighborhood (Table 5). In SSP245, neighborhood weights are determined by comparing the area of land use change to the original land use type's area. In SSP585, the weight for built-up land is set at 1, whereas weights for other land types are reduced, reflecting a 50% higher conversion rate from built-up land between 2010 and 2020. In SSP119, The weight assigned to forest land was raised by 50% in contrast to SSP245, while weights for other land uses variedly decreased. These changes are based on the proportion of forest land converted to other types between 2010 and 2020.

Table 5. Neighborhood weight parameters for three scenarios.

Scenario	Croplands	Forests	Grasslands	Water Body	Built-Up Lands	Barren
SSP245	0.50	0.15	0.58	0.96	0.91	0.05
SSP585	0.41	0.05	0.57	0.95	1.00	0.05
SSP119	0.44	0.23	0.54	0.89	0.62	0.04

3.5. Risk Assessment of Water Supply and Demand

WANG [37] developed a method for evaluating regional risks related to ecosystem service supply and demand using the following formula:

$$R_{(x)} = WY_{(x)}/WD_{(x)} \quad (7)$$

where $WY_{(x)}$ and $WD_{(x)}$ represent the pixel x's water supply and demand, and $R_{(x)}$ denotes the ratio. If $R_{(x)} = 0$, water services are no longer provided in those areas. If $0 < R_{(x)} < 1$, the regional water supply is insufficient to meet demand. If $R_{(x)} > 1$, there is an adequate water supply. Additionally, the change trend in the ratio is determined as follows:

$$R_{tr} = R_m - R_n \quad (8)$$

where R_m and R_n are the ratios in years m and n (n < m), respectively, and R_{tr} is the difference between them. If R_{tr} is below 0, it indicates a decreasing trend; on the contrary, it indicates remaining constant or increasing. Additionally, the water supply and demand trends show absolute changes, calculated as follows:

$$S_{tr} = WY_m - WY_n, D_{tr} = WD_m - WD_n \quad (9)$$

where WY_m, WY_n, WD_m, and WD_n represent the values of supply and demand for corresponding years, while S_{tr} and D_{tr} indicate the changes. If S_{tr} or D_{tr} is negative, it indicates

a decline; if positive, it shows an increasing trend. The risk is then categorized into seven levels, as shown in Table 6.

Table 6. Risk ranking of water ecosystem service.

Grade Code	Risk Grade	Water Supply-Demand Ratio	Water Trend of Supply-Demand Ratio	Trend of Water Supply and Demand
I	Safe	$1 \leq R$	$R_{tr} \geq 0$	-
II	Vulnerable	$1 \leq R$	$R_{tr} < 0$	-
III	Undersupplied	$0 < R < 1$	$R_{tr} \geq 0$	$S_{tr} \geq 0$, $D_{tr} < 0$
IV	Dangerous	$0 < R < 1$	$R_{tr} \geq 0$	$S_{tr} < 0$, $D_{tr} < 0$ or $S_{tr} \geq 0$, $D_{tr} \geq 0$
V	Endangered	$0 < R < 1$	$R_{tr} < 0$	$S_{tr} < 0$, $D_{tr} < 0$ or $S_{tr} \geq 0$, $D_{tr} \geq 0$
VI	Critically endangered	$0 < R < 1$	$R_{tr} < 0$	$S_{tr} < 0$, $D_{tr} \geq 0$
VII	Extinct/Dormant	$R = 0$	-	-

4. Results

Focusing on the Hanjiang River basin, the experiment has three parts: analyzing historical changes in water supply and demand, which identifies their distribution and alignment; projecting future changes under different scenarios, which forecasts supply and demand based on various SSP-RCP scenarios; and assessing associated risks.

4.1. Characteristics of Historical Evolution in Water Supply and Demand

4.1.1. Characteristics of Historical Evolution in Water Supply

The water supply remained stable, increasing from north to south and west to east in 2000–2020 (Figure 5), mirroring precipitation patterns. The annual water yield sharply decreased from 643.43 $\times$ 10^8 m^3/a to 540.65 $\times$ 10^8 m^3/a in 2000–2010 with a decrease of 15.97%, and then rebounded to 629.50 $\times$ 10^8 m^3/a in 2010–2020. High water yield areas were primarily located in Wuhan City Circle, Central East, and Northeast Hubei Province. Conversely, the lowest water yields were observed in Baoji, Luoyang, Sanmenxia, and Shangluo cities. Generally, built-up lands mainly show high water yield, whereas forest generally exhibits low water yield.

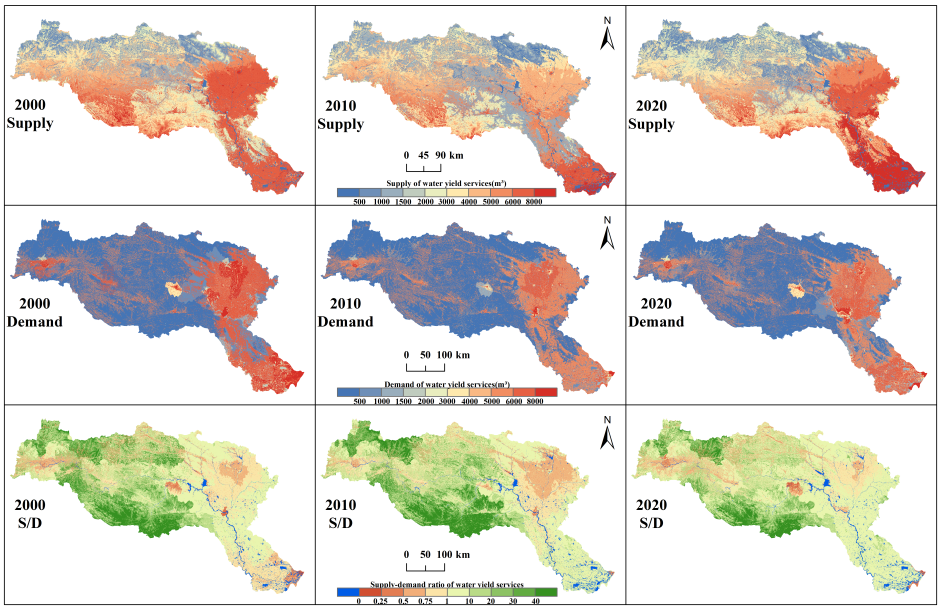


Figure 5. Distribution and correspondence of water supply and demand, 2000–2020.

4.1.2. Characteristics of Historical Evolution in Water Demand

High-demand areas, aligned with the distribution of cropland, are notably concentrated in the Wuhan Urban Circle, Nanyang, and Xiangfan cities (Figure 5). The annual water demand declined from 44,467 million m^3 to 33,859 million m^3 in 2000–2010, and then increased to 37,755,396 million m^3 in 2010–2020, of which Nanyang City, Xiangfan City, and Wuhan City had the highest water demand. Local spatial differences in demand are very obvious, with the water demand of cultivated land in the eastern part of the country far exceeding that of forested and grassland in the western region. In Nanyang City, for example, whose croplands are widely spread, the average annual demand in Nanyang city will be 36.77×10^4 m^3/km^2 in 2020, while in Shiyan City, whose forests and grasslands constitute 53% of the total area, the average annual demand will be only 12.24×10^4 m^3/km^2.

4.1.3. Water Supply and Demand Matching Study

Figure 5 depicts that the northeast, west, and southeast regions have a lower supply-demand ratio, whereas the southwest and north regions exhibit a higher ratio. For example, Ankang City, Shiyan City, and the Shennongjia Forestry Area, which are predominantly covered by forest and grassland, exhibit a higher supply-demand ratio. In terms of temporal variations, 27.06% of the research area had a ratio below 1, indicating a water shortage where supply fell short of demand in 2000 and then decreased to 23.96% in 2000–2010, and further decreased to 17.76% in 2010–2020. The region that is water-scarce continues to shrink. In addition, the overall supply-demand ratio shows an upward trend from 1.447 to 1.667 from 2000–2020.

4.2. Water Supply and Demand Predictions

4.2.1. LUCC Simulation Results and Accuracy Verification

To visually demonstrate the LUCC prediction results, we compared the 2020 land use predictions obtained from data from 2000 to 2010 with the actual values in Figure 6. The predictions closely match the actual values, yielding a Kappa coefficient of 0.851, which confirms the model's reliability for simulating LUCC in the research area in the future.

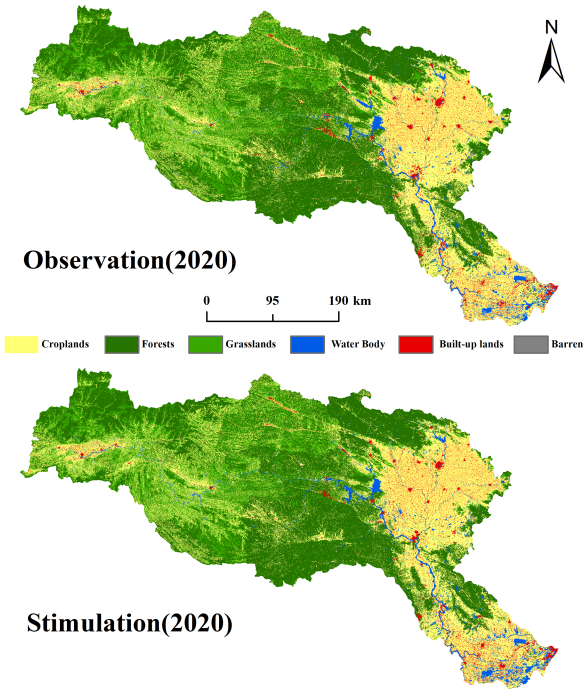


Figure 6. Comparison of land use simulations in 2020.

4.2.2. LUCC Simulation Under Multiple Scenarios

Figure 7 illustrates the consistent spatial patterns. Southeastern Nanyang City and eastern Xiangfan City contain large expanses of cropland. Forests and grasslands are prevalent in Shiyan City, Shennongjia Forest District, northern Hanzhong City, and southern Baoji City. built-up land is concentrated in Wuhan City Circle, Xiangfan City center, key urban areas in Nanyang City, and central Hanzhong City.

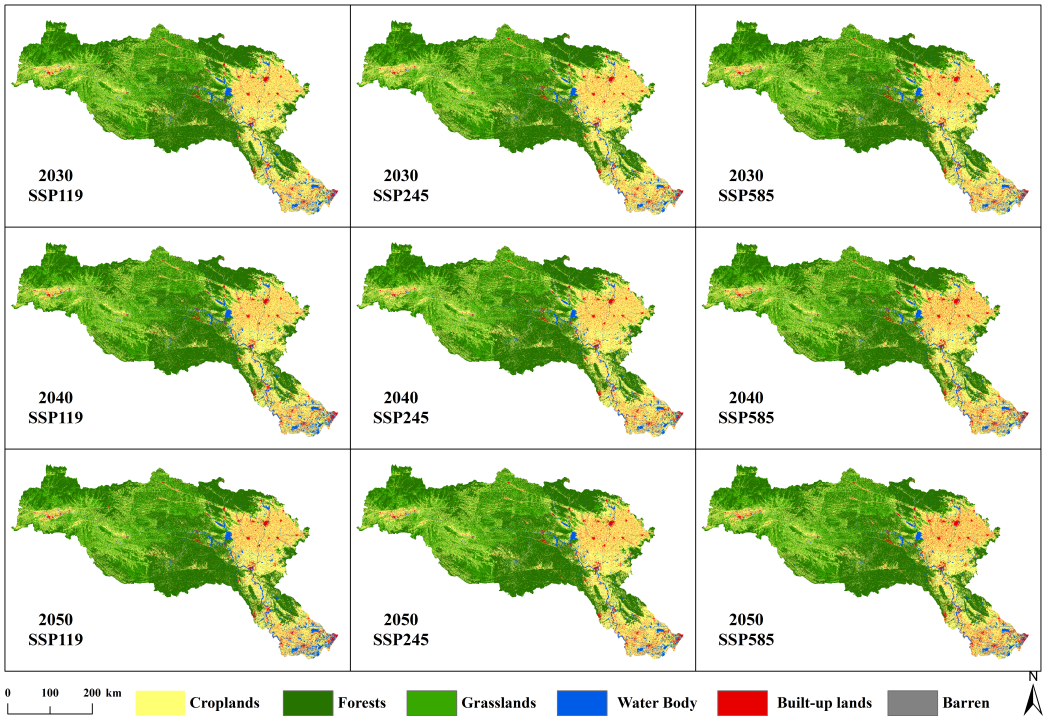


Figure 7. LUCC distribution under three scenarios in the Hanjiang River Basin from 2030 to 2050.

Figure 8 shows the change in major land use types' area, revealing their temporal characteristics. Compared to 53,451.69 km^2 in 2020, the cultivated land area slightly decreases to 52,815.42 km^2 and 51,565.27 km^2 by 2050 under SSP245, a 3.53% reduction. SSP585 and SSP119 show larger declines of 5.45% and 9.36%, respectively. In 2030–2050, woodland and grassland under the SSP585 and SSP245 scenarios remain roughly stable, while forest and grassland show a greater tendency to increase under the SSP119 scenario. From 2030 to 2050, the built-up land area, which was 5139.86 km^2 in 2020, increases under all three scenarios. The expansion rates are 38.80 km^2/year for SSP245, 79.99 km^2/year for SSP585, and 33.67 km^2/year for SSP119, and such expansion under SSP585 significantly encroaches on more cropland than the other two scenarios.

4.2.3. Water Supply and DEMAND Prediction

According to Figures 9 and 10, water supply will be adequate to meet demand from 2030 to 2050, with a spatial distribution pattern similar to historical trends. Water supply is more abundant in the southeast and less available in the north-central region. Despite minimal changes in land use type across 3 scenarios, significant variations in average annual rainfall and actual evapotranspiration create notable differences in water production patterns. Figure 10 illustrates that water demand is highest in major urban centers and extensively cultivated areas in the east, with lower levels centrally.



Figure 8. Changes in major land use types' area, 2030–2050.

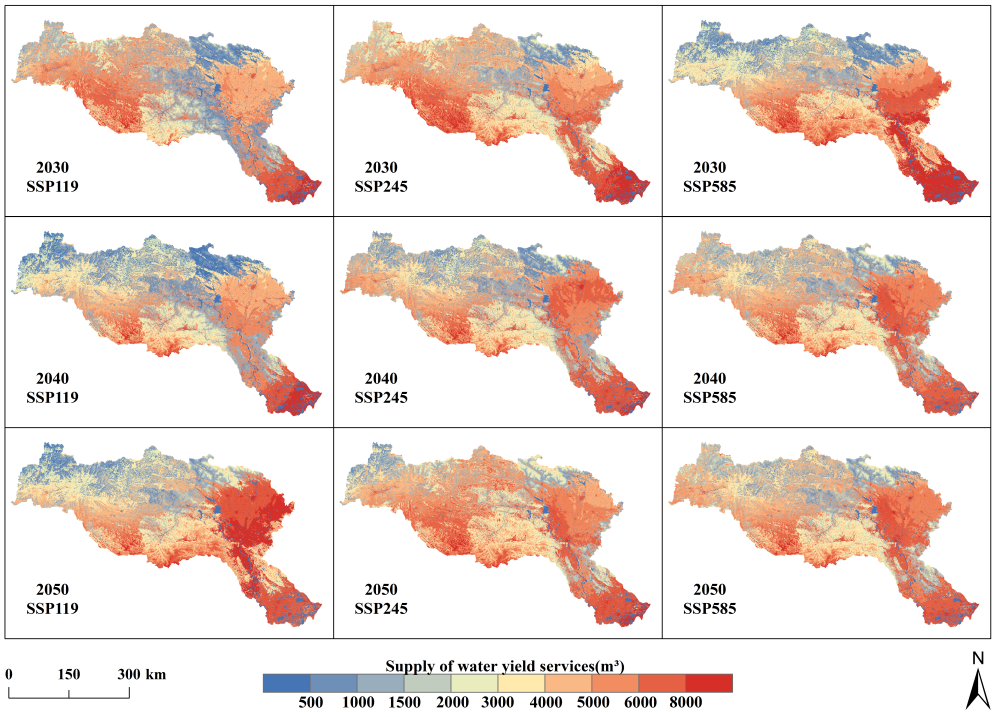


Figure 9. Projected water supply under three scenarios, 2030–2050.

From Figure 11, Tables 7 and 8, we can observe that water supply initially decreases before increasing. Under the SSP245 baseline scenario, the supply of produced water changes from 629,500.6 million m^3 in 2020 to 69,113.41 million m^3 in 2050, which is an enhancement of about 9.79%, the largest enhancement; the supply of water for SSP119 and SSP585 scenarios is also enhanced by 6.06% and 0.49%, respectively; In terms of water demand, under the SSP119 scenario, the demand continues to decrease from 37,755.40 mil-

lion m^3 in 2020 to 28,127.94 million m^3 in 2050, a decrease of 25.5%, and the decrease in water demand also amounts to 21.50% and 22.29% in SSP245 and SSP585, respectively.

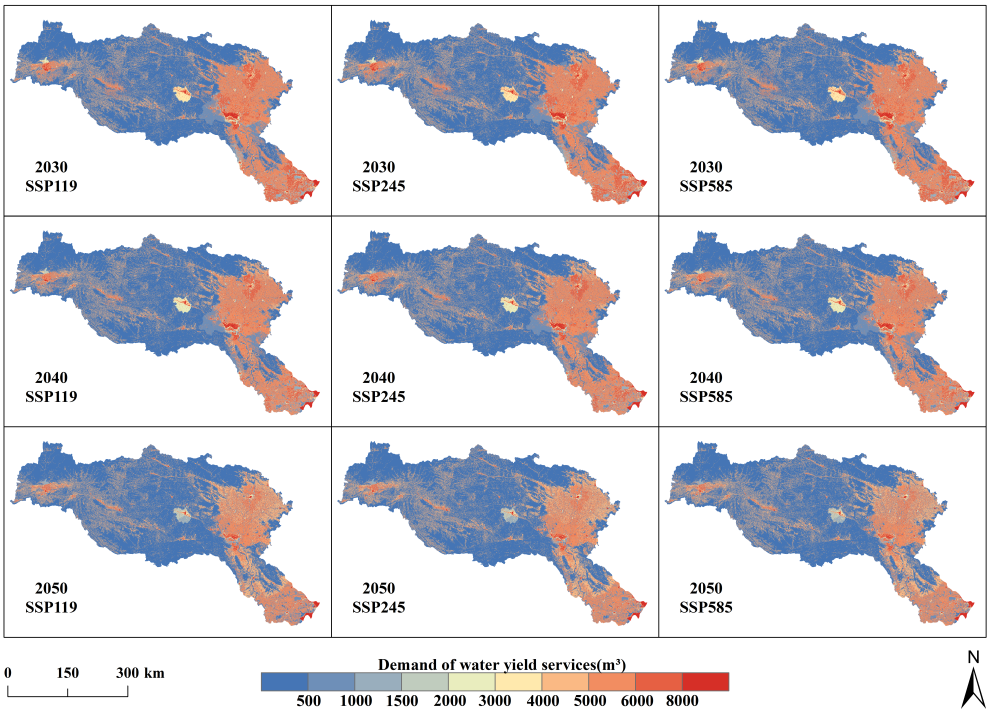


Figure 10. Projected water demand under three scenarios, 2030–2050.

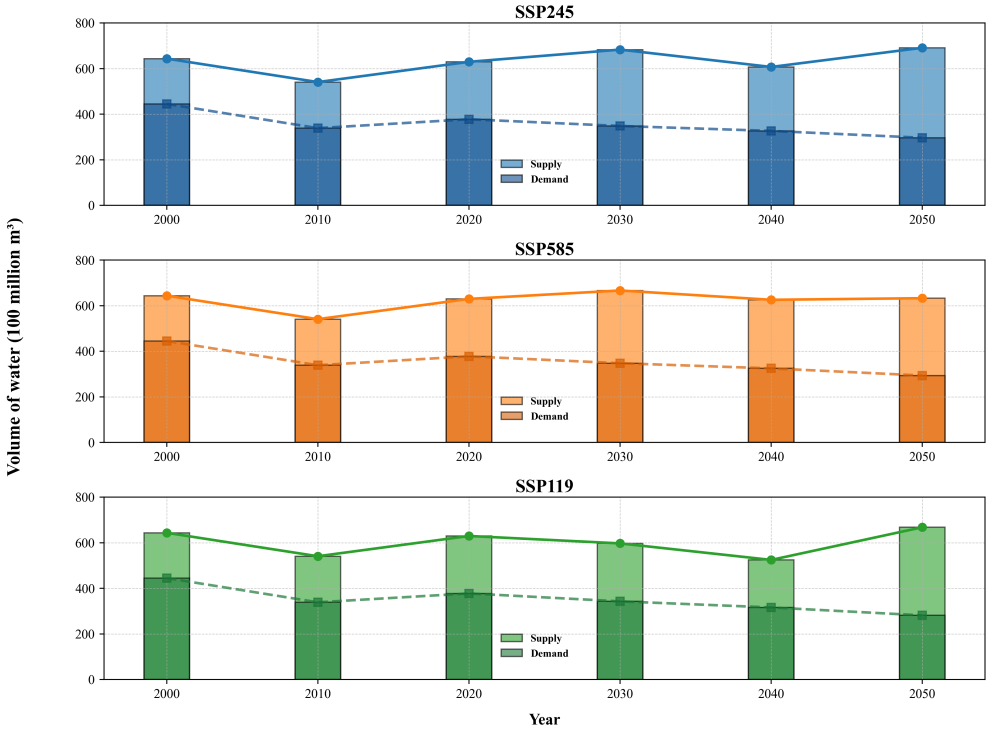


Figure 11. Total water supply and demand under three scenarios, 2000–2050.

Table 7. Water supply under three scenarios (100 million m^3), 2000–2050.

Scenario	2000	2010	2020	2030	2040	2050
SSP245	643.4306	540.6482	629.5006	683.0743	606.951	691.1341
SSP585	-	-	-	666.402	625.5377	632.5587
SSP119	-	-	-	596.9615	524.4701	667.6671

Table 8. Water demand under three scenarios (100 million m^3), 2000–2050.

Scenario	2000	2010	2020	2030	2040	2050
SSP245	444.6661	338.5953	377.5540	348.0393	326.3853	296.3443
SSP585	-	-	-	347.3112	324.7161	293.4152
SSP119	-	-	-	342.6850	315.9838	281.2794

From Figure 12a, it is evident that built-up land has the highest average water supply. however, it is lowest for the forest. For example, in 2030, the average water supply for built-up land is 0.779 m^3/m^2, while that for forested land is only 0.221 m^3/m^2. Water supply decreases to some extent in all three scenarios from 2030 to 2040, and the SSP 119 scenario shows the largest decrease, with a decrease of about 16.69% relative to 2040. This is because the scenario has the lowest average annual rainfall among the three scenarios in 2040 and the largest area of forested land under this scenario.

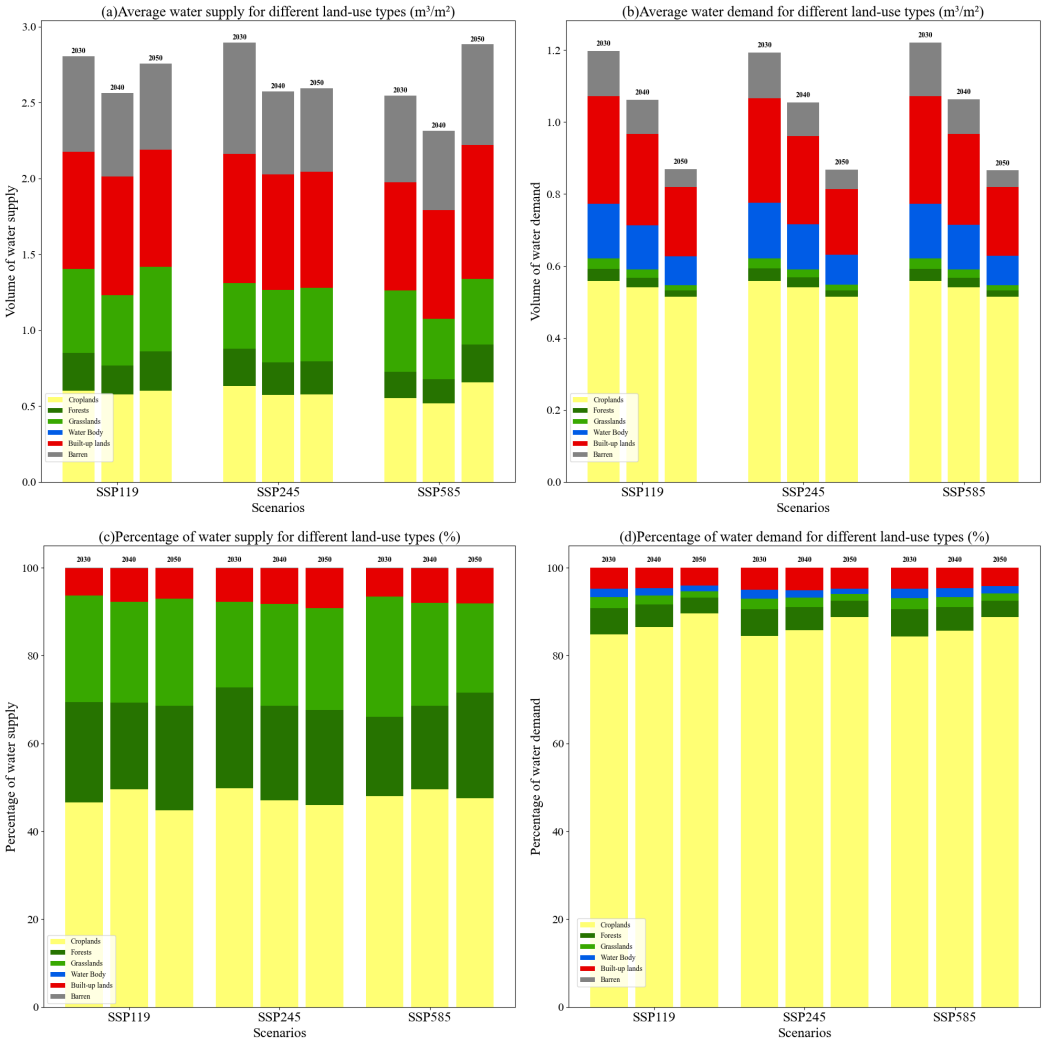


Figure 12. 6 Land use types' average water supply/demand and share, 2030–2050.

The continuous decline in water demand from 2020 to 2050 is largely due to land use changes. Figure 12b shows that in 2030, the average water demand for arable land is 0.558 m^3/m^2, compared to 0.296 m^3/m^2 for built-up land. The total water demand decreases as arable land is converted to built-up land. Figure 12d indicates that cropland accounts for over 80% of the total water demand, so reducing cropland lowers the overall demand. Additionally, the indicator of water consumption of 10,000 CNY GDP has gradually declined, and since this study uniformly uses the weighted average value of the indicator of the current year for all regions, the predicted value of water demand is especially drastically reduced for industries in regions with slow economic development.

4.2.4. Risk Assessment of Water Supply and Demand

As shown in Figure 13 below, from 2030 to 2050, under the three scenarios:

(1) The proportion of areas with a rating of Safe (I) generally displays an upward trend. In SSP119, although the area of endangered (V) is the largest among the three scenarios in 2030, amounting to 14.83%, the proportion of V and VI (high-risk areas) decreases to the lowest in 2050, only 0.51%, and the proportion of its safe (I) area reaches 83.12%.
(2) The vulnerable (II) areas are primarily situated in Hubei Province, with agriculture and building land as land use categories.
(3) The areas in insufficient supply (III) and dangerous (IV) are mainly located in the cultivated areas of Hanzhong, Ankang, and Shangluo. The proportion of undersupplied (III) and hazardous (IV) areas of SSP119, SSP245, and SSP585 scenarios rises from 3.72% to 7.52%, rises from 4.48% to 4.85%, and decreases from 9.86% to 7.58%, with few changes observed from 2030 to 2050, respectively.
(4) High-risk areas V and VI are primarily located in Nanyang City's cropland, which is flat, with extensive cultivated land and a large population, with relatively more water demand requirements, and therefore at somewhat higher risk again. Similarly, the proportion of the area in this region gradually decreases in all scenarios, with the area at endangered risk (V) decreasing from 8.82% in 2030 to 2.50% in 2040 under the SSP245 scenario, with the area of decreasing risk located mainly in the northeastern cropland area of Nanyang City, and the area of endangered risk decreasing slightly to 2.21% in 2050, but the area shifts from Xiangfan City to Nanyang City.

In summary, the risk here will be mitigated under future scenarios, especially under the SSP119 scenario, where the supply and demand situation is most optimistic.

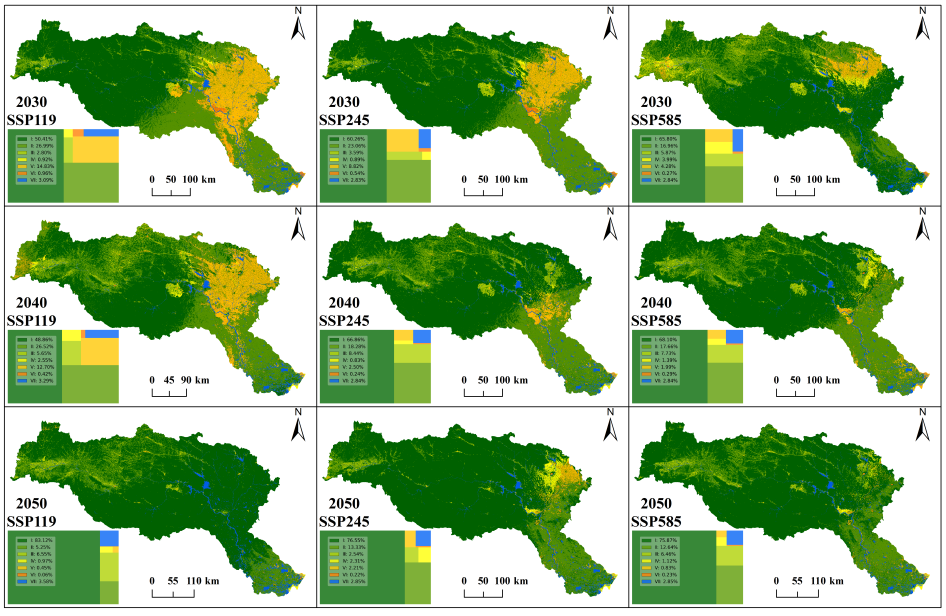


Figure 13. The supply-demand risk of water under three scenarios, 2030–2050.

5. Discussion

This section consists of two parts. First, we explore the spatial heterogeneity of water supply and demand, its drivers, and use a heat map to illustrate how LUCC affects the supply of water yield services. The second part presents our suggestions for water resource allocation in the Hanjiang River Basin based on our findings.

5.1. Exploration of Spatial Heterogeneity in Water Supply and Demand and Drivers Thereof

5.1.1. Analysis of Spatial Autocorrelation

Characteristics of water supply and demand from 2000 to 2020 were analyzed through spatial autocorrelation (Moran's I) at the sub-basin level using ArcGIS 10.8. All global Moran's I indices had *p*-values that exceeded the 0.1% significance level test. Specifically, the average Moran's I indices were 0.258 for supply and 0.288 for demand, indicating a significant global positive spatial correlation between water supply and demand, with clear clustering patterns.

The analysis tool (Getis-OrdGi*) was then used to realize the cold hotspot analysis. Figure 14 illustrates the geographic layout of cold hotspots for water supply and demand, reflecting a clear match, and more hotspots of demand in the Northeast region compared with hotspot distribution of supply. Temporally, the hotspot areas of water production service supply in the southeast expanded and the confidence level increased from 2000 to 2020, indicating that the clustering phenomenon became more and more significant, while the distribution of hotspots of demand did not change significantly.

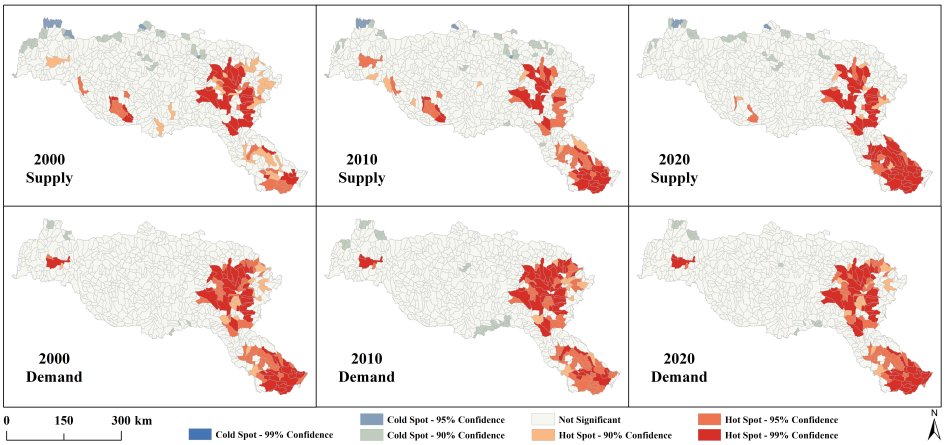


Figure 14. Distribution of hot and cold spots of water supply and demand.

5.1.2. Water Supply and Demand Drivers Analysis

Geodetector assesses the spatial variability of a dependent variable by examining the similarity between the spatial distributions of independent and dependent variables. A higher spatial similarity indicates a stronger influence. The explanatory power of each driver on spatial heterogeneity is represented by the q-value, ranging from 0 to 1, with higher values signifying stronger influence. Additionally, Geodetector can evaluate the interaction effect of two drivers on the same subject's spatial heterogeneity.

We used water supply and demand data from 2000, 2010, and 2020 as dependent variables, respectively, and applied Geodetector to identify key factors driving their spatial heterogeneity. Land use type, average annual temperature and precipitation, average annual actual evapotranspiration (calculated by InVEST water yield module), soil moisture content, elevation, slope, GDP, and population were selected as the driving factors (X1–X9). Then use ArcGIS 10.8 to create a fishing net and cropped it to obtain 17,316 sample points covering the study area for analysis. The average of factor explanatory power of three years was taken to produce a factor interaction heat map (Figure 15).

(1) The one-way detector shows that all nine factors significantly impact the water supply, with land use type, annual average actual evapotranspiration, and annual average rainfall being the most influential, explaining 59%, 47%, and 40% of the variation, respectively. Figure 15a indicates that the combined effects of any two factors surpass the impact of individual factors, with the strongest interactions between land use type and mean annual rainfall, and between precipitation and evapotranspiration, both at 96%. This confirms that land use type drives spatial patterns in water yield, while climate factors, though weak independently, gain significance when interacting with other variables.

(2) Figure 15b shows that land use type explains 81% of the spatial heterogeneity in water demand within the Hanjiang River Basin, indicating it has the greatest impact on this variability. This is an inevitable result of the adoption of the quota method for calculating water demand in this study because, in terms of water for agricultural irrigation, all rasters with the land use type of cropland are regarded as needing to be irrigated.

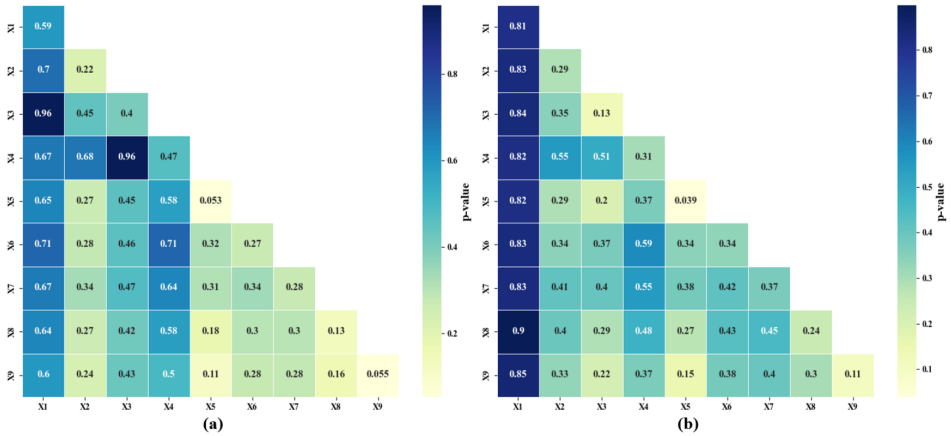


Figure 15. Detection of factor interaction of water supply (**a**)/demand (**b**).

5.1.3. How LUCC Affects Water Supply and Demand

Figure 16a reveals that the cropland has decreased significantly and transformed into other types of land. Specifically, cropland is mainly transformed into built-up land (1569.16 km^2), forest (1092.88 km^2), grassland (934.38 km^2), and water bodies (654.56 km^2). Forest was mainly transformed into cropland (877.26 km^2) and grassland (586.02 km^2), while cropland (739.44 km^2) and forest (888.98 km^2) were the main destinations for converted grassland. Built-up land grew significantly from 3996.05 km^2 to 5139.86 km^2, a 28.62% increase, highlighting the rising demand driven by urbanization.

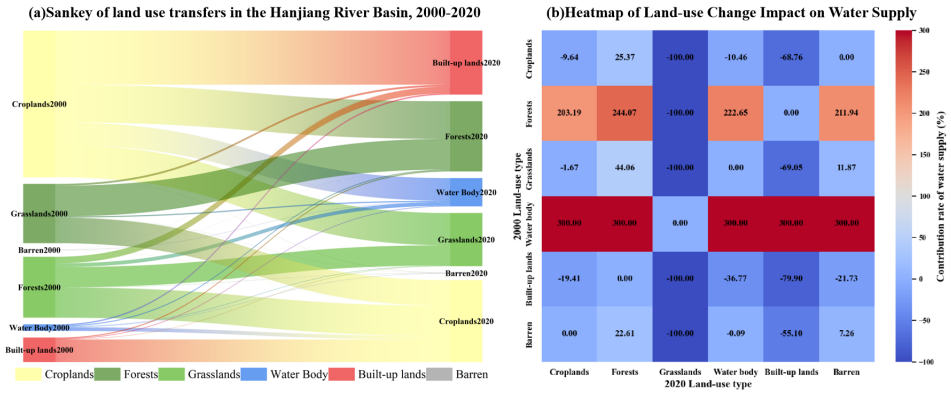


Figure 16. LUCC Sankey (**a**) and Heat map of LUCC's contribution to water supply (**b**).

Since LUCC is used to calculate water demand, its impact on demand will not be further analyzed. To further understand the intrinsic mechanism of such changes, we calculate water supply ensuring only LUCC differs between 2000 and 2020. Figure 16b shows that the contribution of LUCC to water supply varies significantly, as analyzed in detail below:

(1) Water bodies in the Hanjiang River Basin yield minimal water due to high evaporation rates exceeding rainfall. Consequently, the contribution from changing all other land use types into water bodies is considered fully diminished, and the reverse conversion is unquantifiable.
(2) In vegetated areas, water supply ranks as forest, grassland, and cropland in ascending order. Figure 16a shows that converting forest to others each had a significant positive impact on water supply, increasing it by 211.94% for cropland, 222.65% for grassland, and 244.07% for built-up land. This may be due to the higher soil permeability in the forest where the root system can effectively trap precipitation and the dense canopy with its huge transpiration can trap more precipitation and reduce the surface runoff, which is in line with the previous findings demonstrated in Figure 12a.
(3) In built-up land, converting other land use types to this type will enhance water supply because of the lowest vegetation cover, which reduces evapotranspiration after rainfall and increases runoff.

Overall, forest reductions and built-up land expansions notably increase the water supply, as supported by earlier studies [38]. Future land use management should pay attention to improve water resource efficiency and allocation.

5.2. Suggestions for Water Resource Allocation in the Hanjiang River Basin

The water supply and demand hotspots are well-aligned, with the ratio surpassing 1.5 and a surplus water yield of over 200×10^8 m^3. By 2020, water shortage areas have decreased to less than 20%, mainly concentrated in northeastern Nanyang City. To address this, surplus water from the basin should be redistributed. The Danjiangkou area in Shiyan City, with ample water yield, can alleviate water shortages in Nanyang City and nearby regions via the South-to-North Water Transfer Central Route Project. So our results can verify the reasonableness of the site selection and route of the existing projects, and combined with other hydrological elements, such as upstream and downstream runoff study and prediction, can also provide specific recommendations for the subsequent planning of the amount of water transfer.

6. Conclusions

Integrating multi-source geo-environmental data with basin water resources coordination improves our insights into water supply and demand risks, offering more targeted recommendations for water resource allocation and land use management. we draw the following conclusions about the Hanjiang River Basin:

(1) The patterns of LUCC are similar for the three scenarios from 2030 to 2050, with varying levels of decrease for cropland and significant growth of built-up areas, with increases of 6.77% to 19.65% (SSP119), 7.66% to 22.65% (SSP245), and 15.88% to 46.69% (SSP585), respectively, in the three scenarios relative to 2020.
(2) The future supply and demand trends for the three scenarios of produced water services are similar, and the overall supply and demand risks are all on a downward trend. Water demand continues to decline, and by 2050, the water demand of the 3 scenarios will decrease by 96.275×10^8 t, 81.210×10^8 t, and 84.13×10^8 t relative to 2020, respectively; while supply decreases from 2030 to 2040 and rises from 2040 to 2050.
(3) Both water supply and demand distributions exhibit spatial correlation, and the distribution of hotspots is similar. The water supply and demand are well-matched, with an overall supply-demand ratio greater than 1.5.

(4) LUCC can either increase or decrease water yield. built-up land provides more water supply compared to other land types, while forest land has the lowest average water supply. Limiting land use type conversions can enhance the water supply.

We estimate population and GDP under different scenarios by adjusting baseline data from the LUCC perspective using a linear regression approach. However, accuracy significantly decreases for predictions beyond 2050, suggesting the need for authoritative datasets for extended forecasts. Additionally, predicting irrigation water consumption per mu of cropland shows poor accuracy, indicating that integrating rainfall, soil moisture, and other factors into optimized models could improve predictions.

Author Contributions: H.X.: overall research design and paper writing; Y.Y. and H.D.: topic and structure design; X.Z.: review and editing. All authors have reviewed and approved the final version of the manuscript.

Funding: This research was supported by the National Natural Science Foundation of China, project "Research on the Adaptability of Natural-Social Supply and Demand of Water Resource Systems Based on Behavioral Game Theory" (Project No. 41200881).

Institutional Review Board Statement: Not applicable.

Informed Consent Statement: Not applicable.

Data Availability Statement: Data will be made available on request.

Acknowledgments: The authors greatly acknowledge the Resource and Environmental Science and Data Platform and National Earth System Science Data Center for providing the data used in this study.

Conflicts of Interest: The authors declare no conflicts of interest.

References

1. Bishop, C.; Rivard, B.; de Souza Filho, C.; van der Meer, F. Geological remote sensing. *Int. J. Appl. Earth Obs. Geoinf.* **2018**, *64*, 267–274. [CrossRef]
2. Qiu, L.; Xia, W.; Wei, S.; Hu, H.; Yang, L.; Chen, Y.; Zhou, H.; Hu, F. Collaborative management of environmental pollution and carbon emissions drives local green growth: An analysis based on spatial effects. *Environ. Res.* **2024**, *259*, 119546. [CrossRef] [PubMed]
3. Wang, F.; Xiang, L.; Leung, K.S.Y.; Elsner, M.; Zhang, Y.; Guo, Y.; Pan, B.; Sun, H.; An, T.; Ying, G.; et al. Emerging contaminants: A One Health perspective. *Innovation* **2024**, *5*, 100612. [CrossRef] [PubMed]
4. Zhao, X.; Xia, N.; Li, M. Dynamic monitoring of urban renewal based on multi-source remote sensing and POI data: A case study of Shenzhen from 2012 to 2020. *Int. J. Appl. Earth Obs. Geoinf.* **2023**, *125*, 103586. [CrossRef]
5. Sun, Z.; Zhong, Y.; Wang, X.; Zhang, L. Identifying cropland non-agriculturalization with high representational consistency from bi-temporal high-resolution remote sensing images: From benchmark datasets to real-world application. *ISPRS J. Photogramm. Remote Sens.* **2024**, *212*, 454–474. [CrossRef]
6. Wang, N.; Li, W.; Tao, R.; Du, Q. Graph-based block-level urban change detection using Sentinel-2 time series. *Remote Sens. Environ.* **2022**, *274*, 112993. [CrossRef]
7. Zhao, T.; Wang, S.; Ouyang, C.; Chen, M.; Liu, C.; Zhang, J.; Yu, L.; Wang, F.; Xie, Y.; Li, J.; et al. Artificial intelligence for geoscience: Progress, challenges and perspectives. *Innovation* **2024**, *5*, 00691. [CrossRef]
8. Wang, L.; Zuo, B.; Le, Y.; Chen, Y.; Li, J. Penetrating remote sensing: Next-generation remote sensing for transparent earth. *Innovation* **2023**, *4*, 100519. [CrossRef]
9. Wang, S.; Han, W.; Zhang, X.; Li, J.; Wang, L. Geospatial remote sensing interpretation: From perception to cognition. *Innov. Geosci.* **2024**, *2*, 100056. [CrossRef]
10. Wang, S.; Han, W.; Huang, X.; Zhang, X.; Wang, L.; Li, J. Trustworthy remote sensing interpretation: Concepts, technologies, and applications. *ISPRS J. Photogramm. Remote Sens.* **2024**, *209*, 150–172. [CrossRef]
11. Han, W.; Zhang, X.; Wang, Y.; Wang, L.; Huang, X.; Li, J.; Wang, S.; Chen, W.; Li, X.; Feng, R.; et al. A survey of machine learning and deep learning in remote sensing of geological environment: Challenges, advances, and opportunities. *ISPRS J. Photogramm. Remote Sens.* **2023**, *202*, 87–113. [CrossRef]
12. Guan, D.; Deng, Z.; Zhou, L.; Fan, X.; Yang, W.; Peng, G.; Zhu, X.; Zhou, L. How can multiscenario flow paths of water supply services be simulated? A supply-flow-demand model of ecosystem services across a typical basin in China. *Sci. Total Environ.* **2023**, *893*, 164770. [CrossRef] [PubMed]
13. Pei, H.; Liu, M.; Shen, Y.; Xu, K.; Zhang, H.; Li, Y.; Luo, J. Quantifying impacts of climate dynamics and land-use changes on water yield service in the agro-pastoral ecotone of northern China. *Sci. Total Environ.* **2022**, *809*, 151153. [CrossRef] [PubMed]

14. Xia, J.; Dong, Y.; Zou, L. Developing socio-hydrology: Research progress, opportunities and challenges. *J. Geogr. Sci.* **2022**, *32*, 2131–2146. [CrossRef]
15. Deng, C.; Zhu, D.; Nie, X.; Liu, C.; Zhang, G.; Liu, Y.; Li, Z.; Wang, S.; Ma, Y. Precipitation and urban expansion caused jointly the spatiotemporal dislocation between supply and demand of water provision service. *J. Environ. Manag.* **2021**, *299*, 113660. [CrossRef]
16. Dong, Y.; Zou, L.; Xia, J.; Xu, P.; Wang, C.; Zuo, L.; Liu, C. Quantitative analysis of human-water system coevolution incorporating community perceptions: A case study of Wuhan City, China. *J. Hydrol. Reg. Stud.* **2024**, *53*, 101809. [CrossRef]
17. Yifru, B.A.; Chung, I.M.; Kim, M.G.; Chang, S.W. Assessing the Effect of Land/Use Land Cover and Climate Change on Water Yield and Groundwater Recharge in East African Rift Valley using Integrated Model. *J. Hydrol. Reg. Stud.* **2021**, *37*, 100926. [CrossRef]
18. Daneshi, A.; Brouwer, R.; Najafinejad, A.; Panahi, M.; Zarandian, A.; Maghsood, F.F. Modelling the impacts of climate and land use change on water security in a semi-arid forested watershed using InVEST. *J. Hydrol.* **2021**, *593*, 125621. [CrossRef]
19. Wang, F.; Liu, J.; Qin, G.; Zhang, J.; Zhou, J.; Wu, J.; Zhang, L.; Thapa, P.; Sanders, C.J.; Santos, I.R.; et al. Coastal blue carbon in China as a nature-based solution towards carbon neutrality. *Innovation* **2023**, *4*, 5100481. [CrossRef]
20. Li, D.; Wu, S.; Liu, L.; Liang, Z.; Li, S. Evaluating regional water security through a freshwater ecosystem service flow model: A case study in Beijing-Tianjian-Hebei region, China. *Ecol. Indic.* **2017**, *81*, 159–170. [CrossRef]
21. Wang, Q.; Guan, Q.; Sun, Y.; Du, Q.; Xiao, X.; Luo, H.; Zhang, J.; Mi, J. Simulation of future land use/cover change (LUCC) in typical watersheds of arid regions under multiple scenarios. *J. Environ. Manag.* **2023**, *335*, 117543. [CrossRef] [PubMed]
22. Luo, J.; Fu, H. Constructing an urban cooling network based on PLUS model: Implications for future urban planning. *Ecol. Indic.* **2023**, *154*, 110887. [CrossRef]
23. Liu, X.; Liu, Y.; Wang, Y.; Liu, Z. Evaluating potential impacts of land use changes on water supply–demand under multiple development scenarios in dryland region. *J. Hydrol.* **2022**, *610*, 127811. [CrossRef]
24. Zhou, Y.; Guo, S.; Hong, X.; Chang, F.J. Systematic impact assessment on inter-basin water transfer projects of the Hanjiang River Basin in China. *J. Hydrol.* **2017**, *553*, 584–595. [CrossRef]
25. Cui, Y.; Liu, J.; Xu, X.; Dong, J.; Li, N.; Fu, Y.; Lu, S.; Xia, H.; Si, B.; Xiao, X. Accelerating Cities in an Unsustainable Landscape: Urban Expansion and Cropland Occupation in China, 1990–2030. *Sustainability* **2019**, *11*, 2283. [CrossRef]
26. Liang, X.; Guan, Q.; Clarke, K.C.; Liu, S.; Wang, B.; Yao, Y. Understanding the drivers of sustainable land expansion using a patch-generating land use simulation (PLUS) model: A case study in Wuhan, China. *Comput. Environ. Urban Syst.* **2021**, *85*, 101569. [CrossRef]
27. Liu, X.; Liang, X.; Li, X.; Xu, X.; Ou, J.; Chen, Y.; Li, S.; Wang, S.; Pei, F. A future land use simulation model (FLUS) for simulating multiple land use scenarios by coupling human and natural effects. *Landsc. Urban Plan.* **2017**, *168*, 94–116. [CrossRef]
28. Chen, X.; Lin, S.; Tian, J.; Wang, Y.; Ye, Y.; Dong, S.; Gong, X.; Lin, Q.; Zhu, L. Simulation study on water yield service flow based on the InVEST-Geoda-Gephi network: A case study on Wuyi Mountains, China. *Ecol. Indic.* **2024**, *159*, 111694. [CrossRef]
29. Project, N.C. *InVEST 3.14.2 User's Guide*; Stanford University: Stanford, CA, USA; University of Minnesota: Minneapolis, MN, USA; Chinese Academy of Sciences: Beijing, China; The Nature Conservancy: Arlington, VA, USA; World Wildlife Fund: Washington, DC, USA; Stockholm Resilience Centre: Stockholm, Sweden, 2022.
30. Bagstad, K.; Villa, F.; Johnson, G.; Voigt, B. ARIES–Artificial Intelligence for Ecosystem Services: A guide to models and data, version 1.0. *ARIES Rep. Ser.* **2011**, *1*,102.
31. Ray, S.; Lama, A.; Mishra, P.; Biswas, T.; Sankar Das, S.; Gurung, B. An ARIMA-LSTM model for predicting volatile agricultural price series with random forest technique Image 1. *Appl. Soft Comput.* **2023**, *149*, 110939. [CrossRef]
32. Yue, W.; Qin, C.; Su, M.; Teng, Y.; Xu, C. Simulation and prediction of land use change in Dongguan of China based on ANN cellular automata—Markov chain model. *Environ. Sustain. Indic.* **2024**, *22*, 100355. [CrossRef]
33. Liang, X.; Guan, Q.; Clarke, K.C.; Chen, G.; Guo, S.; Yao, Y. Mixed-cell cellular automata: A new approach for simulating the spatio-temporal dynamics of mixed land use structures. *Landsc. Urban Plan.* **2021**, *205*, 103960. [CrossRef]
34. Taylor, K.E.; Stouffer, R.J.; Meehl, G.A. An overview of CMIP5 and the experiment design. *Bull. Am. Meteorol. Soc.* **2012**, *93*, 485–498. [CrossRef]
35. O'Neill, B.C.; Tebaldi, C.; Van Vuuren, D.P.; Eyring, V.; Friedlingstein, P.; Hurtt, G.; Knutti, R.; Kriegler, E.; Lamarque, J.F.; Lowe, J.; et al. The scenario model intercomparison project (ScenarioMIP) for CMIP6. *Geosci. Model Dev.* **2016**, *9*, 3461–3482. [CrossRef]
36. Peng, S.; Ding, Y.; Wen, Z.; Chen, Y.; Cao, Y.; Ren, J. Spatiotemporal change and trend analysis of potential evapotranspiration over the Loess Plateau of China during 2011–2100. *Agric. For. Meteorol.* **2017**, *233*, 183–194. [CrossRef]
37. Wang, H.; Liu, G.; Li, Z.; Zhang, L.; Wang, Z. Processes and driving forces for changing vegetation ecosystem services: Insights from the Shaanxi Province of China. *Ecol. Indic.* **2020**, *112*, 106105. [CrossRef]
38. Aghsaei, H.; Mobarghaee Dinan, N.; Moridi, A.; Asadolahi, Z.; Delavar, M.; Fohrer, N.; Wagner, P.D. Effects of dynamic land use/land cover change on water resources and sediment yield in the Anzali wetland catchment, Gilan, Iran. *Sci. Total Environ.* **2020**, *712*, 136449. [CrossRef]

Disclaimer/Publisher's Note: The statements, opinions and data contained in all publications are solely those of the individual author(s) and contributor(s) and not of MDPI and/or the editor(s). MDPI and/or the editor(s) disclaim responsibility for any injury to people or property resulting from any ideas, methods, instructions or products referred to in the content.